可见光标识：除了第一个都在可见光范畴。
单、多层：1；2
凸起、凹槽：1；2
有无激励源：1 有；2 无；　　　例如类别：单层、凸槽、无源：112

<table>
<tr><td>论文编号</td><td colspan="3">内容整理</td></tr>
<tr><td rowspan="8">1</td><td>类别</td><td colspan="2">112</td></tr>
<tr><td>单元描述</td><td colspan="2">Hybrid circular split ring resonator (h-SRR)
A h-SRR on a square unit cell is adopted as a basic building block for the study of metasurface properties.</td></tr>
<tr><td rowspan="2">结构单元图</td><td>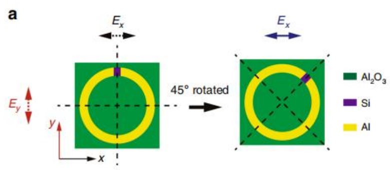
</td><td>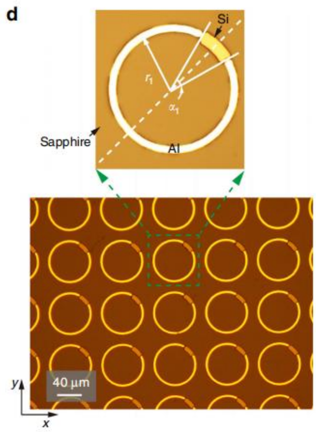
</td></tr>
<tr><td colspan="2">a Schematic illustrations of an anisotropic h-SRR with different configurations relative to the incident electric field polarization.
d Microscopic images of the fabricated h-SRR sample array with a zoomed-in image showing the details of an individual resonator with geometrical parameters (in μm) r1 = 37, α1 = 10°, metal width = 5, and square period = 80</td></tr>
<tr><td rowspan="4">指标</td><td>1 透射共振峰</td><td>2 透射偏振谱</td></tr>
<tr><td>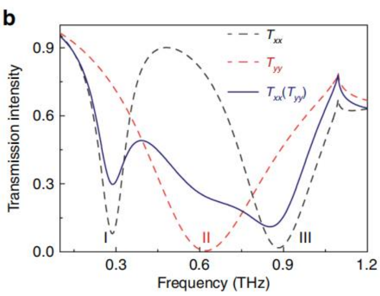
</td><td>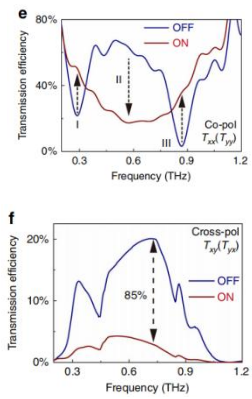
</td></tr>
<tr><td colspan="2">b Simulated transmission intensity spectra of the h-SRR resonator array. All three fundamental modes are simultaneously excited by rotating the h-SRR by 45° relative to the linear incident polarization (solid dark blue line). Intrinsic resonance modes (dashed lines) are induced by orthogonal polarization excitation along the optical axes of the resonator in the transmission spectra
e, f Experimental demonstration of alloptical active control of the anisotropy in terms of mode switching in the co- and cross-polarized transmission spectra; the 85% modulation is on the basis of the OFF state spectrum</td></tr>
<tr><td></td><td></td></tr>
<tr><td></td><td></td><td colspan="2"></td></tr>
</table>

<table>
<tr><td rowspan="9">2</td><td>类别</td><td colspan="2">112</td></tr>
<tr><td>单元描述</td><td colspan="2">The “uncover” metasurface consists of an amorphous 2D array of Ag nanoparticles with a hemispherical shape and an average in-plane diameter near 100 nm</td></tr>
<tr><td rowspan="2">结构单元图</td><td>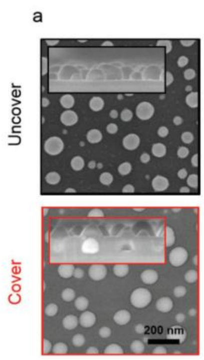
</td><td>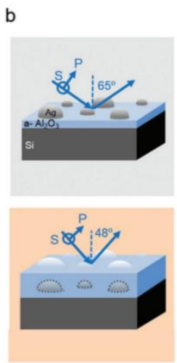
</td></tr>
<tr><td colspan="2">Nanostructure and room-temperature optical properties of the “uncover” and “cover” metasurfaces.
a) Scanning electron images: top-view and cross-section (insets).
b) Configuration of the optical measurements. The orientation of the electric field for s- and p-polarized incident light is denoted as “s” and “p,” respectively.</td></tr>
<tr><td rowspan="5">指标</td><td>1 反射偏振 sp 谱</td><td>2 椭偏振幅系数Ψ</td></tr>
<tr><td>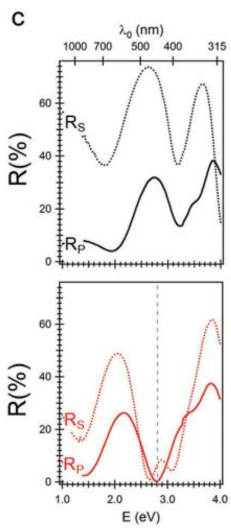
</td><td>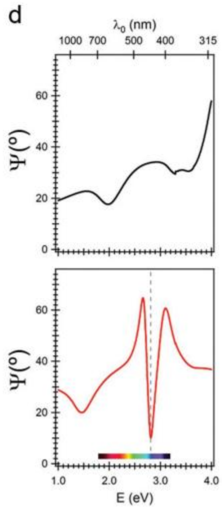
</td></tr>
<tr><td colspan="2">c) Room-temperature specular reflectance spectra for s- and p-polarized light, Rs and Rp, respectively, for an angle of incidence (AOI) of 65° (“uncover” metasurface) and 48° (“cover” metasurface).
d) Room-temperature spectra of the ellipsometric amplitude coefficient Ψ at the same AOIs. The “cover” metasurface shows a sharp drop and near cancelation of Ψ for (AOI = 48°, photon energy E ≈ 2.8 eV) where quasi-darkness conditions are fulfilled.</td></tr>
<tr><td>3 椭偏振幅Ψ</td><td>4 相位系数Δ</td></tr>
</table>

		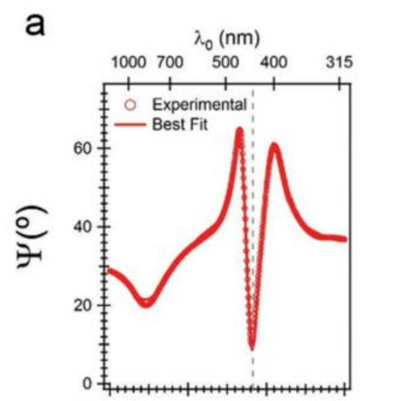 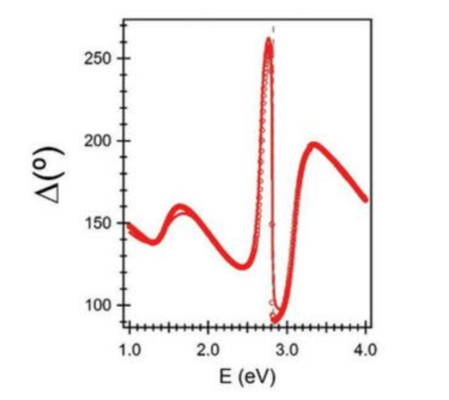
		“Cover” metasurface: reflected light phase jump in quasi-darkness conditions enabled by thin film interference–plasmon resonances hybridization. a) Experimental and best-fit simulated room-temperature spectra of the ellipsometric amplitude and phase coefficients, Ψ and Δ, for an AOI of 48°. An abrupt Δ variation occurs in the quasi-darkness conditions (AOI = 48°, E ≈ 2.8 eV)
3	类别	112
	单元描述	勾型阵列超表面结构产生涡旋光束，该结构可以有效的将圆偏振光和线偏振光转 化为涡旋光束，并在线偏振涡旋光入射的情况下，在多个角度上均可以有效地实现涡旋光束的转化
	结构单元图	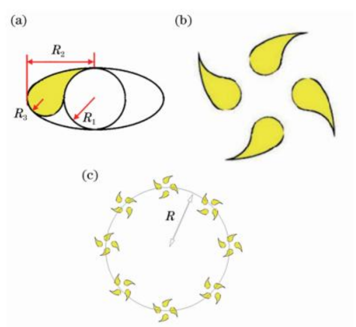
		勾型超表面阵列结构示意图。（a）勾型超表面结构；（b）勾型超表面单元；（c）勾型超表面阵列。 设 定 R1 =75 nm，R2 = 300 nm，R3 = R2 - 2R1 = 150 nm，R =800 nm。金属超表面的厚度 d1 = 100 nm，SiO2 基底的底座厚度 d2 = 300 nm，SiO2 基底的底部到探测面的距离设为 L
	指标	1 超表面阵列的耦合效率曲线
		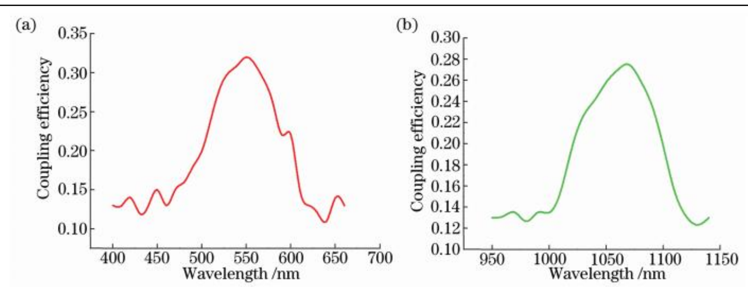

<table>
<tr><td></td><td></td><td colspan="2">（a）原尺寸的超表面结构；（b）横向尺寸放大 1.6 倍，纵向尺寸保持不变后的超表面结构</td></tr>
<tr><td></td><td></td><td></td><td></td></tr>
<tr><td rowspan="9">4</td><td>类别</td><td colspan="2"></td></tr>
<tr><td>单元描述</td><td colspan="2">蛾眼抗反射结构模型</td></tr>
<tr><td rowspan="2">结构单元图</td><td>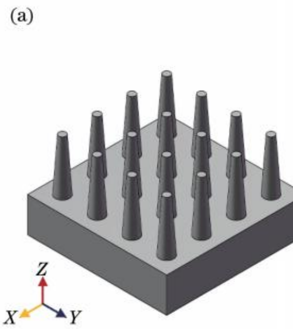
</td><td>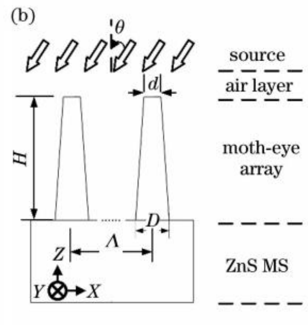
</td></tr>
<tr><td colspan="2">图 1　蛾眼结构理论模型.(a)三维结构模型　　　(b)仿真模型示意图</td></tr>
<tr><td rowspan="5">指标</td><td colspan="2">1 宽光谱透过率与蛾眼结构参数关系曲线图</td></tr>
<tr><td colspan="2">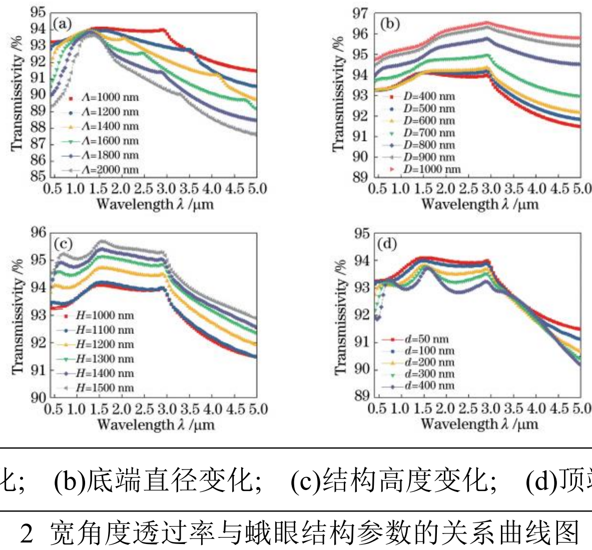
</td></tr>
<tr><td colspan="2">(a)周期变化；(b)底端直径变化；(c)结构高度变化；(d)顶端直径变化</td></tr>
<tr><td colspan="2">2 宽角度透过率与蛾眼结构参数的关系曲线图</td></tr>
</table>

		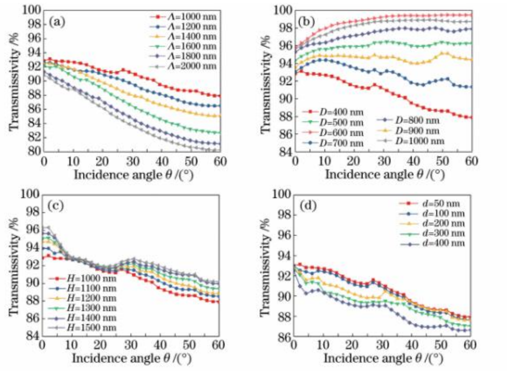
		(a) 周期变化 (D＝４００nm,H ＝１０００nm,d＝５０nm); (b) 底端直径(Λ＝１０００nm,H ＝１０００nm,d＝５０nm); (c) 结构高度变化(Λ＝１０００nm,D＝４００nm,d＝５０nm); (d)顶端直径变化(Λ＝１０００nm,D＝４００nm,H ＝１０００nm)
5	类别	112
	单元描述	梯形结构。单元结构由 SiO2 衬底和高折射率的晶体 Si 纳米柱两部分组成。Si 纳米柱为梯形结构，其俯视图为直角梯形，放置在长方体衬底上表面的中心。高折射率的 Si 柱能够将光能量束缚在设计的结构内，避免相邻单元之间的耦合。通过调整上底 a、下底 b、宽度 t 可以得到 0~2π范围内不连续相位梯度分布。
	结构单元图	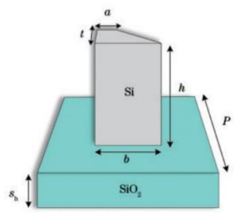
		超透镜的单元结构图
	指标	1 线偏振光入射时的结构参数与透射率相位关系
		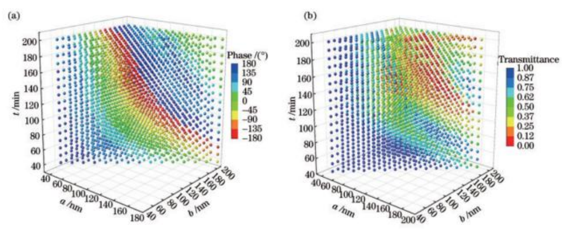
		（a）微元结构参数与相位和 （b）微元结构参数与透射率
		2 圆偏振光入射时的情况
		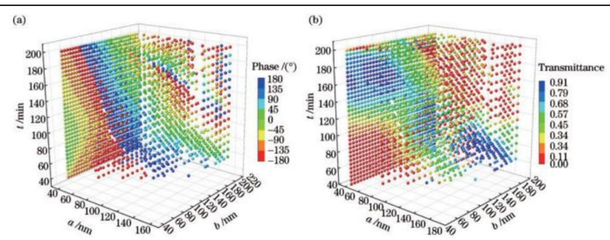

<table>
<tr><td rowspan="4"></td><td rowspan="4"></td><td colspan="2">（a）微元结构参数与相位和（b）微元结构参数与透射率</td></tr>
<tr><td colspan="2">3 两种入射光在不同型号下的透射率和相位</td></tr>
<tr><td>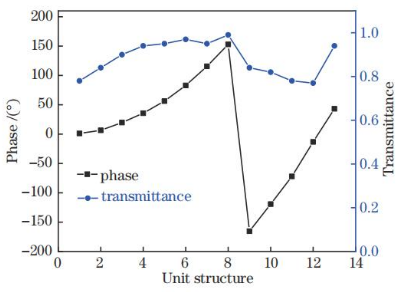</td><td>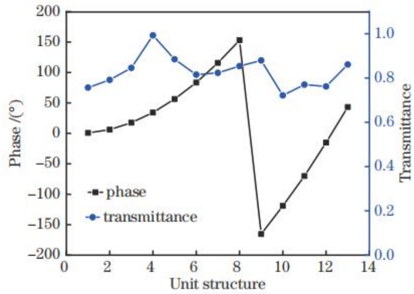</td></tr>
<tr><td>当入射 640 nm 的 TM 波时透射率较高的结构：周期为 200 nm 的单排结构下各个结构的相位和透射率</td><td>在 640 nm 的右旋圆偏振入射下的单排结构：
周期为 200 nm 的单排结构下各个结构的相位和透射率</td></tr>
<tr><td></td><td></td><td></td><td></td></tr>
<tr><td rowspan="7">6</td><td>类别</td><td colspan="2">112</td></tr>
<tr><td>单元描述</td><td colspan="2">介质-金属-介质光栅的一维单周期反射彩色滤光结构</td></tr>
<tr><td rowspan="2">结构单元图</td><td colspan="2">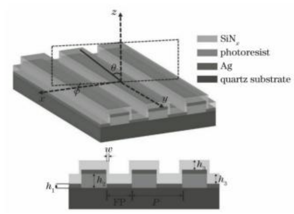</td></tr>
<tr><td colspan="2">当 Ag 膜厚度 h1 为 20nm,光刻胶栅高 h2 为 140nm,介质厚度 h3 为 120nm,介质对光栅横向包裹的宽度 w 为 20nm,周期 P 为 520nm,占空比 F 为 0.4 时,利用时域有限差分(FDTD)算法分析该结构在θ=45°,φ分别为 0°和 90°时的反射特性</td></tr>
<tr><td rowspan="3">指标</td><td colspan="2">1 占空比变化时的反射光谱与优化后反射光谱及其对应颜色</td></tr>
<tr><td colspan="2">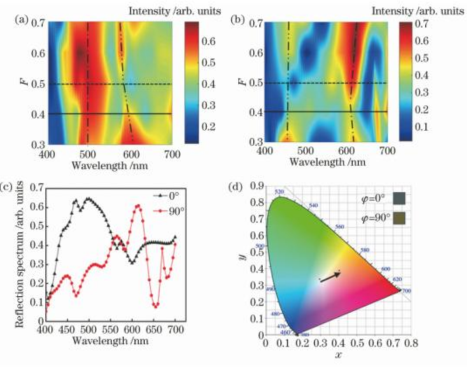</td></tr>
<tr><td colspan="2">(a)φ=0°反射光谱。其中，反射峰的中心波长(长-短线)，次反射峰(长-短-短线)
(b)φ=90°反射光谱;
(c)两个平面优化后的反射光谱;(d)反射光谱对应的 CIE1931 色域图</td></tr>
</table>

<table>
<tr><td></td><td></td><td>2 介质层膜厚变化时的反射光谱与优化后反射光谱及其对应颜色。</td></tr>
<tr><td></td><td></td><td>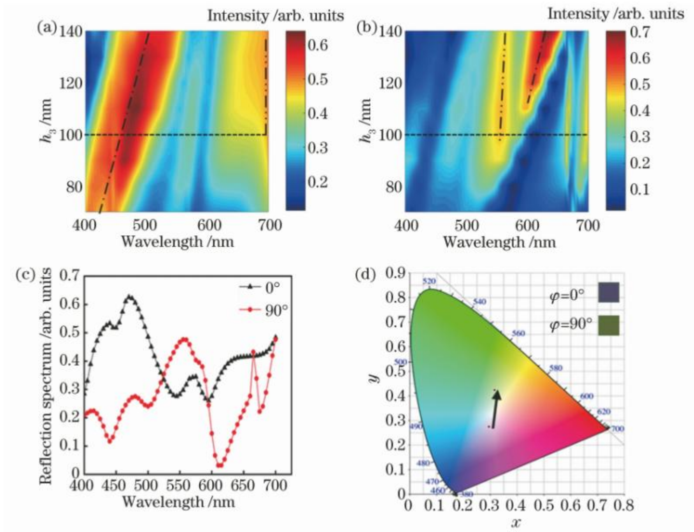
</td></tr>
<tr><td></td><td></td><td>(a)φ=0°反射光谱。其中，反射峰的中心波长(长-短线)，次反射峰(长-短-短线)
(b)φ=90°反射光谱;
(c)两个平面优化后的反射光谱;
(d)反射光谱对应的 CIE1931 色域图</td></tr>
<tr><td></td><td></td><td>3: 介质层折射率变化时，白光 45°倾斜入射下的反射光谱</td></tr>
<tr><td></td><td></td><td>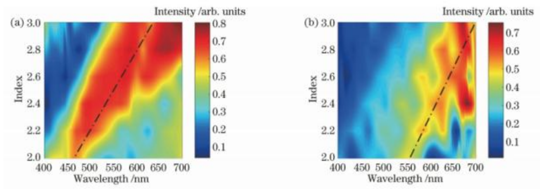
</td></tr>
<tr><td></td><td></td><td>(a)φ=0°反射光谱；反射峰的中心波长(长-短线)，反射峰的峰值和半峰全宽增加,峰值高达 80%
(b)φ=90°反射光谱；中心波长(长-短线)产生红移,反射峰的峰值和半峰全宽增加,峰值高达 70%</td></tr>
<tr><td></td><td></td><td></td></tr>
<tr><td rowspan="3">*7</td><td>类别</td><td>122</td></tr>
<tr><td>单元描述</td><td>In this work, we use multipole meta-atoms that supportnot only ED and MD but also an electric quadrupole (EQ) and a magnetic quadrupole (MQ) to construct an ideal half-wave plate. We propose a multipole meta-atom design consisting of a metallic nanoaperture and a metallic nanorod separated by a perforated dielectric layer. The dimension of the nanorod
(Fig. 1b) and thus the multipole response (Fig. 1c) can be modified by introducing a small air gap between the nanorod and the dielectric spacer separating adjacent meta-atoms</td></tr>
<tr><td>结构</td><td></td></tr>
</table>

<table>
<tr><td rowspan="8"></td><td rowspan="2">单元图</td><td>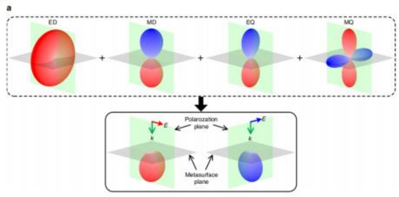
</td><td>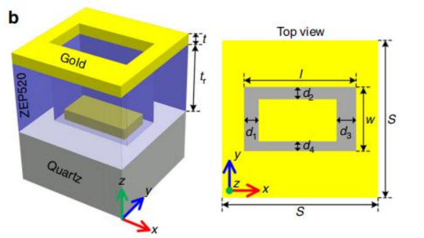
</td></tr>
<tr><td colspan="2">a Schematic showing radiation patterns of ED,MD, EQ, and MQ supported by a multipole meta-atom and their interference scattering for two orthogonal LPs at a specific wavelength in which a π-phase difference exists between the two LPs.
b Schematic showing the designed multipole meta-atom, which consists of a gold nanoaperture and a gold nanorod separated by a perforated ZEP520 layer. In the meta-atom, S = 320 nm, l = 230 nm, w = 130 nm, t = 35 nm, and tr= 180 nm. The multipole response of this meta-atom can be tuned by introducing an air gap between the nanorod and ZEP520 sidewalls, i.e., a noncomplementarity between the nanorod and the nanoaperture. The dimension of the air gap is denoted by d1,2,3,4 in four sides</td></tr>
<tr><td rowspan="6">指标</td><td colspan="2">1 不同辐射模式下的散射截面</td></tr>
<tr><td colspan="2">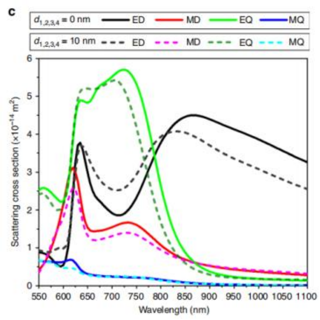
</td></tr>
<tr><td colspan="2">C) Calculated scattering cross sections contributed from each multipole for complementary (solid lines) and noncomplementary (dashed lines) MPMs with a RCP input.</td></tr>
<tr><td colspan="2">2 不同尺寸下的透射光谱</td></tr>
<tr><td colspan="2">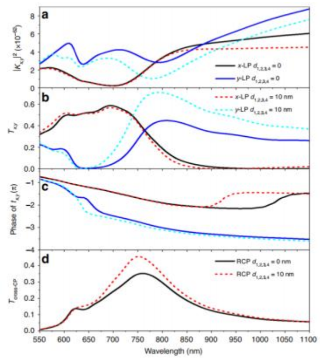
</td></tr>
<tr><td colspan="2">(a)transmittance
(b), and phase of transmission coefficients
(c) with LP inputs, and cross-CP transmittance
(d) with a RCP input for a complementary</td></tr>
</table>

		MPM with d1,2,3,4 = 0 (solid lines) and a noncomplementary MPM with d1,2,3,4 = 10 nm (dashed lines).
		3 模拟交叉圆偏振光的透射幅度和相位
		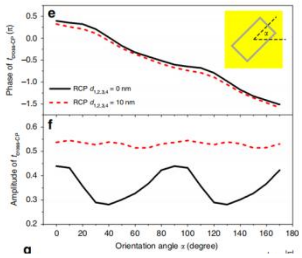
		(e) amplitude (f) of the cross-CP transmission coefficients with a RCP input for metaatoms with different orientations.
8	类别	122
	单元描述	a class of compact slits nano-antennas array in metallic film that lif all these limitations
	结构单元图	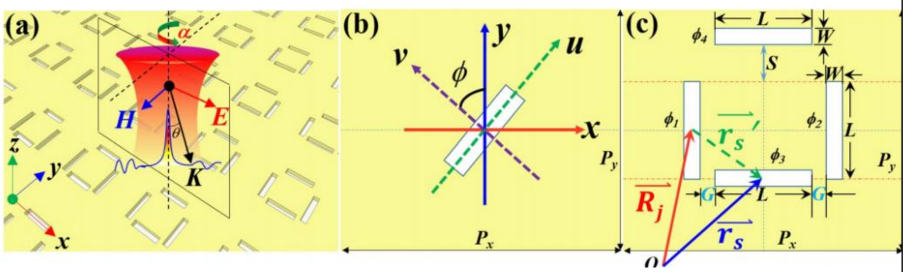
		(a) Schematic of the proposed nanostructures with particular identical rectangular slits. (b) Scheme of the unit cell showing one slit and corresponding coordinates. (c) Coordinate vector and unit cell of the proposed metasurface.
	指标	1 理论透射系数和数值模拟下的反射光谱
		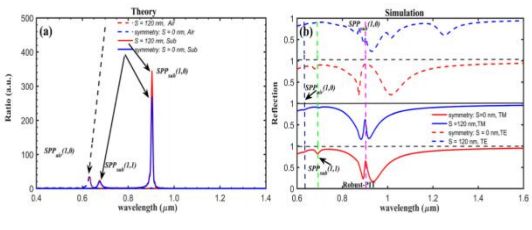
		(a) Teoretic model calculated transmission coefficient at TM (solid-lines)/TE (dashed-lines) incidence for 100×100 periodic unit, (b) numerical simulated refection spectra of the metasurface. “Sub” and “Air” indicate the substrate and upper air interfaces.
		2 横磁波横电波偏振入射下的色散分布

<table>
<tr><td rowspan="4"></td><td rowspan="4"></td><td>
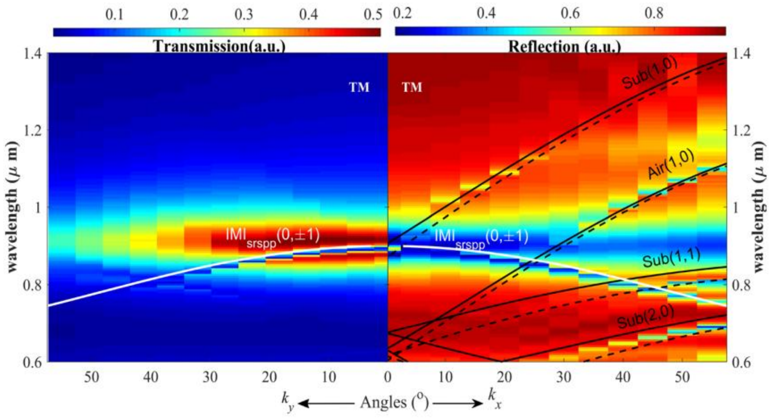

</td></tr>
<tr><td>Figure 5. Calculated dispersion of the system for TM polarization incidence.
Left panel：Calculated transmission spectra dispersion.
Right panel: Calculated refection spectra dispersion. Te superimposed white solid line denotes the calculated dispersion for asymmetry (air–Au–glass) three-layer (insulator–metal–insulator, IMI) wave guide-mode. Te superimposed black lines are the dispersion curves of air and substrate SPP modes (solid lines) and wood anomaly (dashed lines). Robust PIT-like effect is observed.</td></tr>
<tr><td>
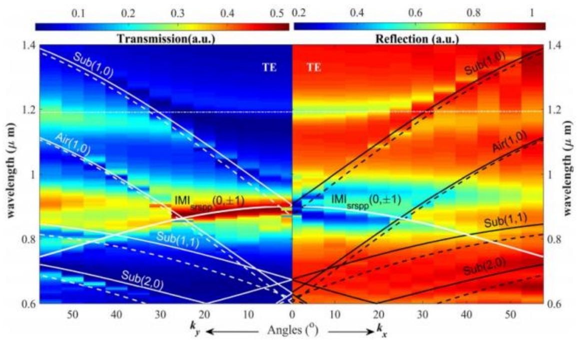

</td></tr>
<tr><td>Figure 6. Calculated dispersion of the system for TE polarization incidence.
Lef panel: Calculated transmission spectra as a function of frequency and in-plane wave vector ky.
Right panel: Calculated refection spectra as a function of frequency and in-plane wave vector kx. Te superimposed white solid line denotes the calculated dispersion curves for SPP Bloch-mode and the asymmetry IMI wave guide-mode.</td></tr>
<tr><td></td><td></td><td></td></tr>
<tr><td rowspan="3">9</td><td>类别</td><td>112</td></tr>
<tr><td>单元描述</td><td>We report on a non-sharp-corner quarter wave plate (NCQW) within the single layer of only 8 nm thickness structured by the Ag hollow elliptical ring array, where the strong localized surface plasmons (LSP) resonances are excited Te Ag layer with the thickness of h is coated on a SiO2 substrate and is shaped to the hollow elliptical ring array.</td></tr>
<tr><td>结构单元</td><td></td></tr>
</table>

<table>
<tr><td rowspan="7"></td><td>图</td><td>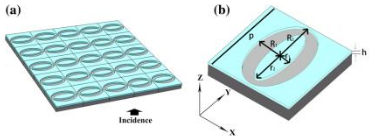
</td></tr>
<tr><td></td><td>Figure 1. Structure of proposed NCQW.
(a) Schematics of the proposed plasmonic metasurface NCQW structure (5×5 units). Te light incidend from the substrate side as the arrow.
(b) One unit of the proposed NCQW structure.</td></tr>
<tr><td rowspan="4">指标</td><td>1 空心环的透射和相位分布</td></tr>
<tr><td>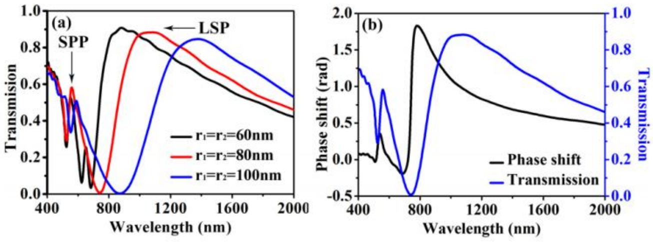
</td></tr>
<tr><td>(a) Te transmission at r1=r2=60 nm, 80 nm and 100 nm, respectively.
(b) the transmission and the phase shif at r1=r2=80 nm. Te other parameters are R1=R2=120 nm, h=8 nm, and p=330 nm.</td></tr>
<tr><td></td></tr>
<tr><td></td></tr>
<tr><td></td><td></td><td></td></tr>
<tr><td rowspan="4">10</td><td>类别</td><td>112</td></tr>
<tr><td>单元描述</td><td>Highly efficient subtractive tri-color filters of cyan, magenta, and yellow with enhanced color purity and robustness have been proposed and realized, by exploiting a silicon-aluminum (Si-Al) hybrid-nanodisk (ND) metasurface atop a Si substrate.</td></tr>
<tr><td rowspan="2">结构单元图</td><td>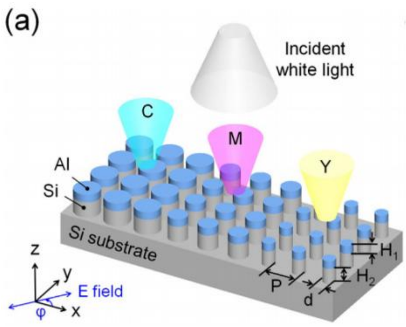

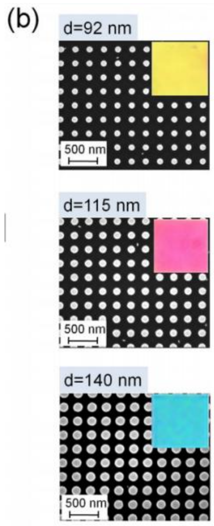
</td></tr>
<tr><td>(a) Schematic configuration.
(b) SEM images of the fabricated color filters with diameters of d=92nm, 115nm, and 140nm for a fixed period of P=240nm, corresponding to yellow, magenta, and cyan, respectively. Inset reveals individual optical microscope</td></tr>
</table>

images produced by the filters.

指标

1 三种区域的反射率比较图

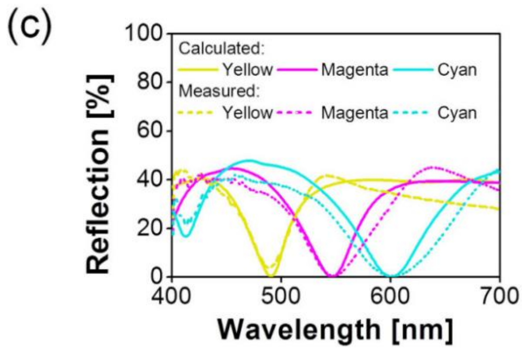

(c) Reflection spectral responses of the CMY devices for normal incidence.

2 直径 d 排列周期 p 对于反射光谱、颜色响应的影响

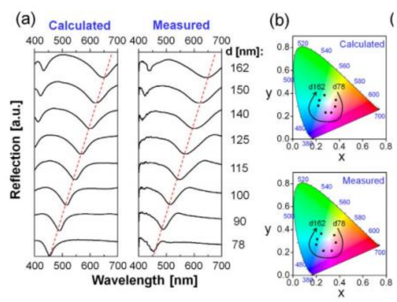

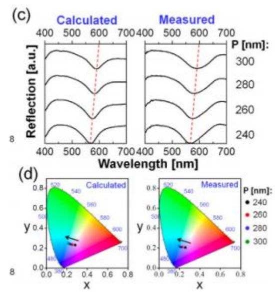

(a) Reflection spectra of the proposed filters with diameters ranging from d=78 to 162nm for a fixed period of P=240nm, with the red dashed line tracing the location of the reflection dip.

(b) Chromaticity coordinates in the CIE 1931 chromaticity diagram corresponding to the spectra depending on the ND diameter.

(c) Reflection spectra in response to the period ranging from 240nm to 300nm for a fixed diameter of d=120nm, with the locus of the reflection dips traced in red dashed line.

(d) Chromaticity coordinates corresponding to the spectra as a function of the period.

3 亮场下的调色板图像和测量的反射光谱

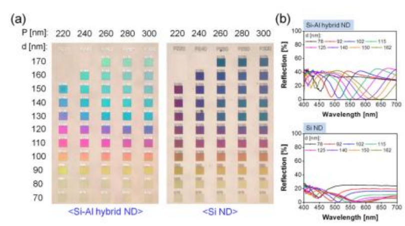

(a) Measured bright-field microscope images of the prepared color palette based on the proposed Si-Al hybrid-ND metasurface and the Si ND case. Each filter consists of NDs with different diameters and periods, having a footprint

<table>
<tr><td></td><td></td><td>of 30×30μm2
(b) measured reflection spectra for the proposed Si-Al hybrid-ND-based filters and the Si ND case, as the diameters increase from 78nm to 162nm for a period of P=240nm.</td></tr>
<tr><td></td><td></td><td>4 反射光谱、共振场分布和反射依赖性的比较</td></tr>
<tr><td></td><td></td><td>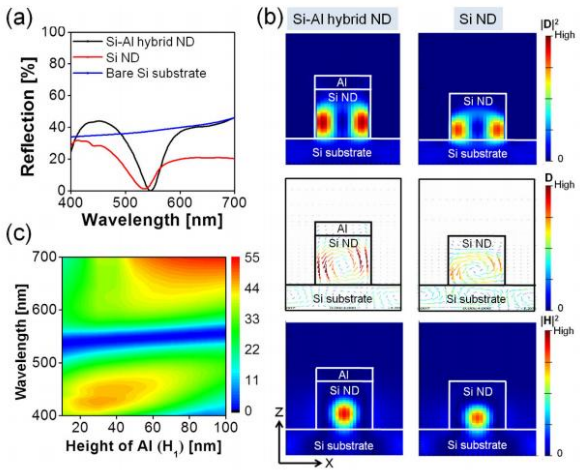
</td></tr>
<tr><td></td><td></td><td>Of proposed color filters on the height of top Al ND.
(a) Calculated reflection spectra for the proposed magenta filter, Si-ND structure, and bare Si substrate.
(b) D-field intensity profile (|D|2) and the corresponding vector plot, and the H-field intensity profile (|H|2) for the proposed filters at resonance, in comparison to the
case of the Si-ND array; here, a set of circular D-field loops develop, whereby they underlie the MD resonance modes for both cases.
(c) Contour map of the reflection spectra of the proposed filters, with the height of the Al
ND ranging from H1=10nm to 100nm.</td></tr>
<tr><td></td><td></td><td></td></tr>
<tr><td rowspan="3">11</td><td>类别</td><td>112</td></tr>
<tr><td>单元描述</td><td>Design of CMOS anti-Hermitian metasurface. The colorsorting metasurface is composed of three types of silicon nanocylinders with different diameters d, patterned into a hexagonal
lattice with a sub-wavelength center-to-center nanocylinder spacing, a, of 220 nm,</td></tr>
<tr><td>结构单元图</td><td>a
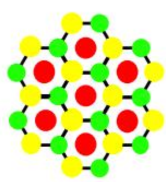
b
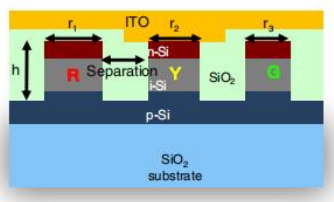
</td></tr>
</table>

<table>
<tr><td rowspan="10"></td><td></td><td>a) Top</td><td>b) side-view schematic of 3-color,2-D array of silicon nanocylinders.</td></tr>
<tr><td rowspan="9">指标</td><td colspan="2">1 三种不同直径的硅纳米柱体的吸收光谱</td></tr>
<tr><td colspan="2">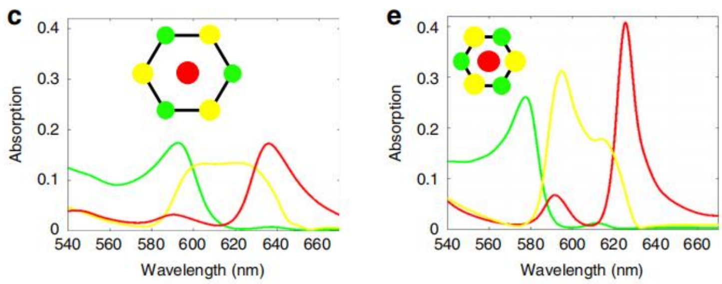
</td></tr>
<tr><td colspan="2">C) 350 nm, mixed coupling condition,
e) 220 nm, anti-Hermitian coupling condition</td></tr>
<tr><td colspan="2">2 三种电流通道下的吸收光谱</td></tr>
<tr><td colspan="2">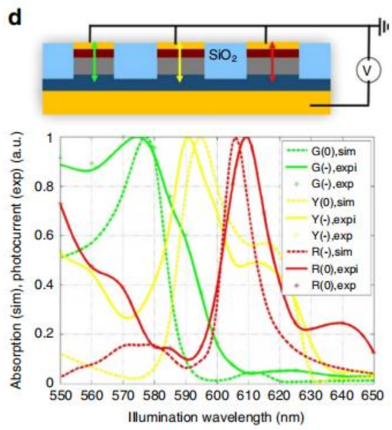
</td></tr>
<tr><td colspan="2">d Combined photocurrent and absorption spectra of all three channels. Legend labels “sim”, “expi”,and “exp” refer to simulated, interpolated experimental, and raw experimental data, respectively.</td></tr>
<tr><td></td><td></td></tr>
<tr><td colspan="2"></td></tr>
<tr><td colspan="2"></td></tr>
<tr><td rowspan="2">12</td><td>类别</td><td colspan="2">112</td></tr>
<tr><td>单元描述</td><td colspan="2">Here, we demonstrated a high-quality 5 GHz optoacoustic vibration and ultrafast optomechanical all-optical manipulation in a sub-5 nm tip-supported nanooptomechanical metasurface (TSNOMS).</td></tr>
</table>

<table>
<tr><td rowspan="5"></td><td>结构单元图</td><td colspan="2">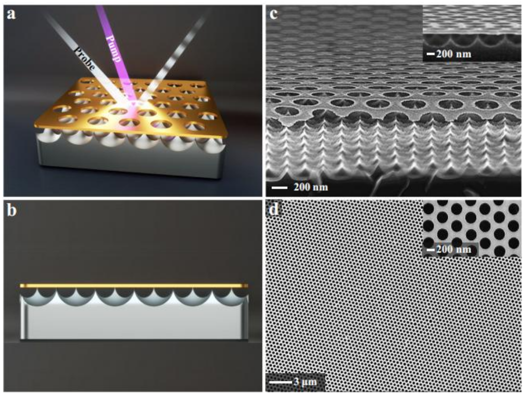

a: Concept image showing the vibrational response of the probe signal through optical excitation of the TSNOMS.
b: Concept image of the TSNOMS.
c, d：SEM image of the TSNOMS.</td></tr>
<tr><td rowspan="4">**指标**</td><td>1 测量和有限元模拟下的反射光谱</td><td>2 纳米尖端和基板各自的反射光谱</td></tr>
<tr><td>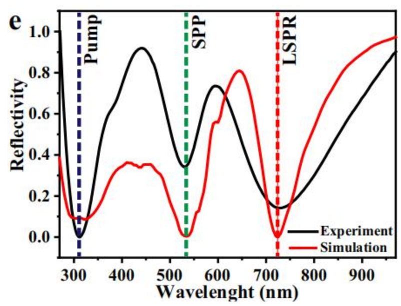
</td><td>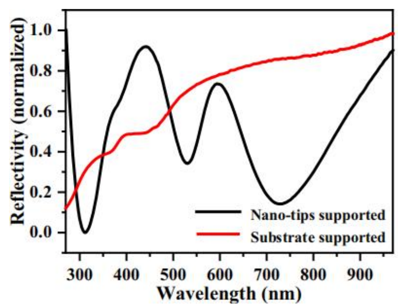
</td></tr>
<tr><td>e Measured reflection spectra of the TSNOMS (black lines) and reflection spectra simulated by the finite element method (red line).</td><td>b Optical reflectance spectra of the optomechanical metasurface supported on a monocrystalline silicon substrate and the silicon nanotip arrays.</td></tr>
<tr><td colspan="2"></td></tr>
<tr><td></td><td></td><td colspan="2"></td></tr>
<tr><td rowspan="3">**13**</td><td>类别</td><td colspan="2">112</td></tr>
<tr><td>单元描述</td><td colspan="2">a planar array of metal nanoparticles—the exact shape of the nanoparticles is not critical—with spatially and directionally controlled spacing.</td></tr>
<tr><td>结构单元图</td><td colspan="2">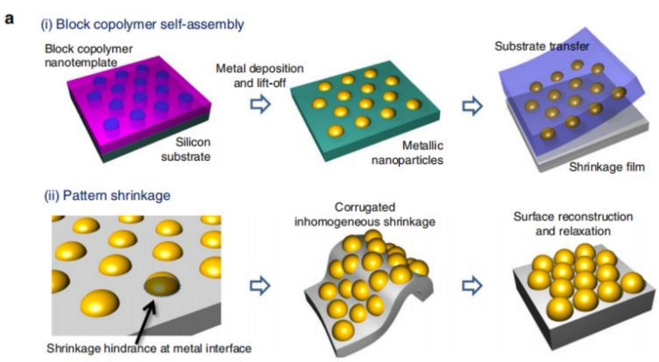

Schematic for metal nanoparticle ensemble preparation by
(i) BCP selfassembly and substrate transfer and</td></tr>
</table>

<table>
<tr><td rowspan="7"></td><td></td><td>(ii) pattern shrinkage</td></tr>
<tr><td rowspan="6">指标</td><td>1 金属纳米颗粒超表面系综收缩前后的透射光谱</td></tr>
<tr><td>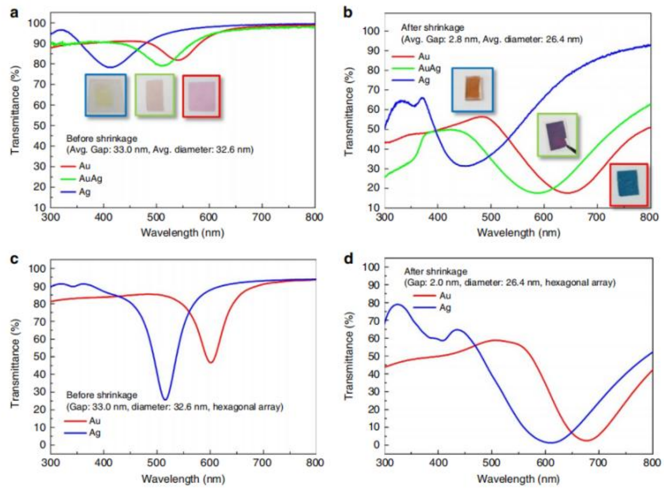
</td></tr>
<tr><td>(a,b) Ultraviolet–vis spectroscopy and photographs of Au, Ag
and Au–Ag alloy nanoparticle ensemble before (a) and after shrinkage (b).
(c,d) Corresponding FDTD transmittance simulations of Au, Ag nanoparticle ensembles</td></tr>
<tr><td>2 不同波长下的折射率和消光系数</td></tr>
<tr><td>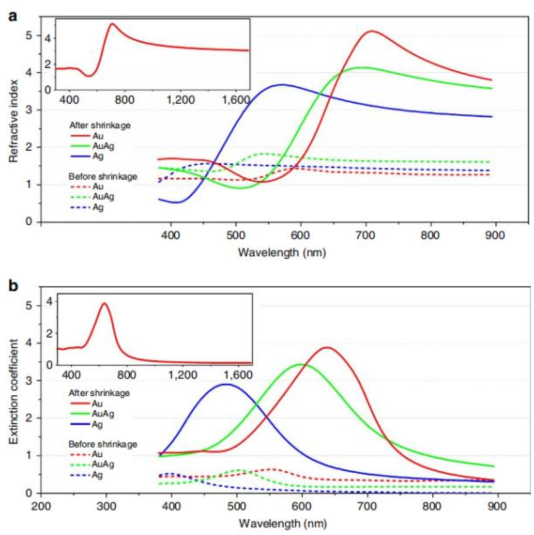
</td></tr>
<tr><td>Ellipsometry measurements of
(a) refractive indices and
(b) extinction coefficients of Au,Ag and Au–Ag alloy nanoparticle ensembles before (dashed line) and after (solid line) pattern shrinkage.</td></tr>
<tr><td></td><td></td><td></td></tr>
<tr><td rowspan="2">14</td><td>类别</td><td></td></tr>
<tr><td>单元描述</td><td>Simultaneous manipulation of reflection spectrum and phase using asymmetric meta-atoms. In this work, we use an asymmetric bar-shaped nanowaveguide which provides two phase modulation principles, i.e.,propagation phase and</td></tr>
</table>

<table>
<tr><td rowspan="9"></td><td></td><td>geometric phase</td></tr>
<tr><td rowspan="2">结构单元图</td><td>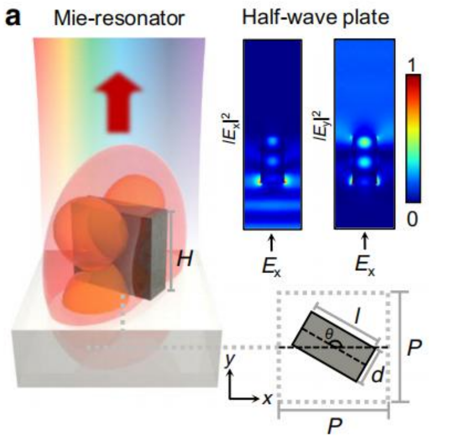
</td></tr>
<tr><td>a： Schematic of the multifunctional meta-atom which acts as a Mie-resonator and a localized half-wave plate. The meta-atom has length l, height H, width d, pitch P, and an in-plane rotation angle of θ.</td></tr>
<tr><td rowspan="6">指标</td><td>1 在 532 nm 处的交叉极化转换效率</td></tr>
<tr><td>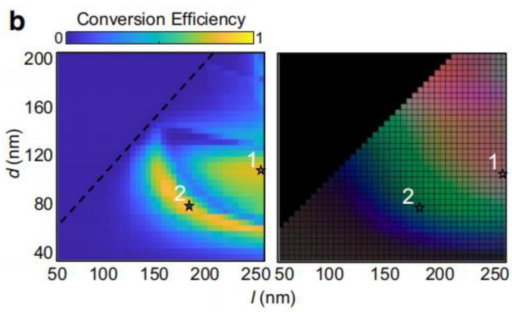
</td></tr>
<tr><td>b Cross-polarization conversion efficiency at 532 nm and color palette of meta-atoms with l from 50 to 250 nm and d from 40 to 200 nm, with H = 350 nm and P = 300 nm.</td></tr>
<tr><td>2 样品的反射光谱</td></tr>
<tr><td>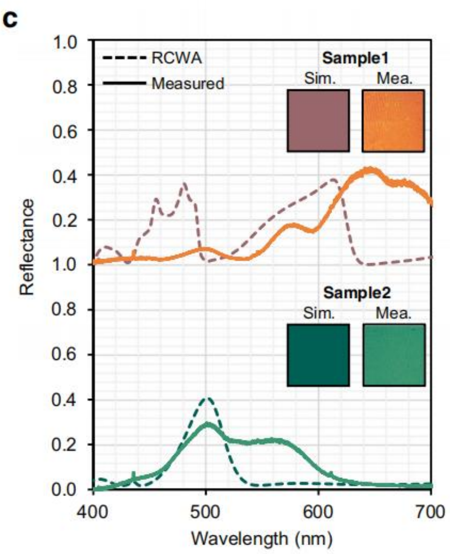
</td></tr>
<tr><td>c Reflection spectra of Samples 1 and 2. Dashed line: RCWA simulation; solid</td></tr>
</table>

<table>
<tr><td rowspan="7"></td><td rowspan="7"></td><td colspan="2">line: experimental measurement. Insets represent the calculated and measured colors of Samples 1 and 2.</td></tr>
<tr><td colspan="2">3 在不同模式下沿 x 轴的交叉散射截面</td></tr>
<tr><td colspan="2">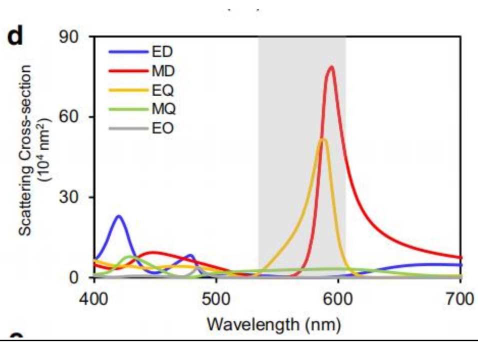
</td></tr>
<tr><td colspan="2">d Multipole decomposition of the scattering response of the meta-atom array in free space under linearly polarized light along the x-axis. The meta-atoms have l = 250 nm, d = 95 nm, H = 350 nm, and P = 300 nm. Gray colored area indicates the regime where the interplay between the strong MD and EQ modes occurs.</td></tr>
<tr><td colspan="2">4 多极矩与 RCWA 模拟的反射率</td></tr>
<tr><td colspan="2">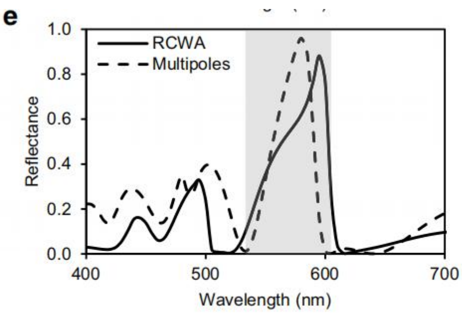
</td></tr>
<tr><td colspan="2">e Comparison between the reflectance retrieved from the multipole moments and RCWA simulation.</td></tr>
<tr><td></td><td></td><td colspan="2"></td></tr>
<tr><td rowspan="3">15</td><td>类别</td><td colspan="2">？2 1</td></tr>
<tr><td>单元描述</td><td colspan="2">In this paper, we introduce a design of electrically controlled EIT metasurface loaded with nematic LC, which allows us to change the spectral resonance response of the metasurface in the NIR region by tuning an external electric field, under an unchanged incident light.</td></tr>
<tr><td>结构单元图</td><td>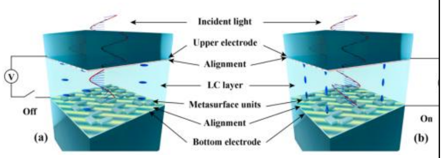
</td><td>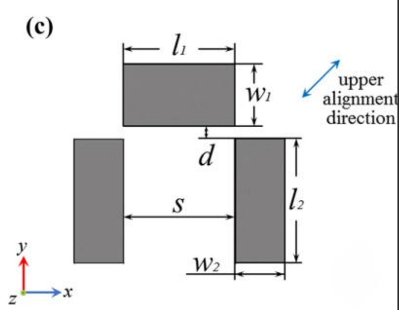
</td></tr>
</table>

		Schematic diagram for the EIT metasurface and LC sections at (a) the “of ” state and (b) the “on” state. (c) Planar structural representation of a metasurface unit.
	指标	1 沿 x 方向偏振光的透射反射率 | 2 在“关”和“开”状态下的 lc-超表面透射光谱
		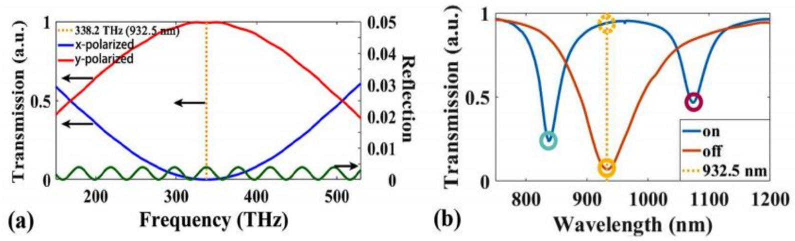
		(a) Conversion for x-polarization incident light. | (b) Spectrum comparison between the “on” and “of ” states.
16	类别	
	单元描述	In this paper, we stretch the use of 12-in. immersion photolithograpy on silicon wafers and subsequent etching processes one step beyond to produce high-quality and high-throughput nanostructural colors that are closer to those done by EBL, thus bringing the technology closer to industrial applications.
	结构单元图	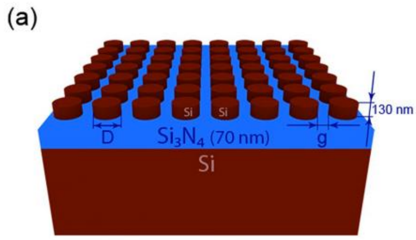
		(a) Schematics of nanostructure design
	指标	1 不同尺寸阵列下的反射光谱（实验、模拟值）——表征颜色
		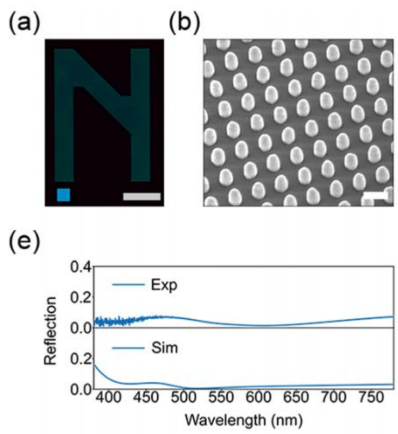 | 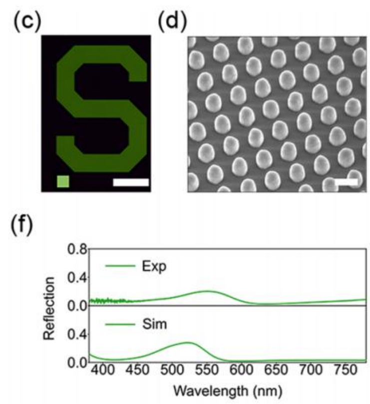

<table>
<tr><td rowspan="2"></td><td rowspan="2"></td><td>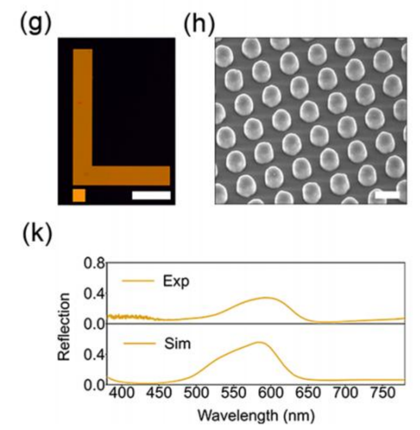
</td><td>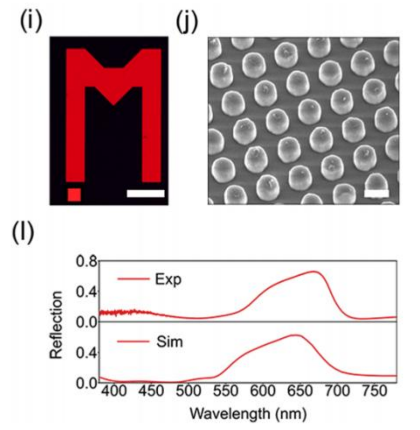
</td></tr>
<tr><td colspan="2"></td></tr>
<tr><td></td><td></td><td colspan="2"></td></tr>
<tr><td rowspan="6">17</td><td>类别</td><td colspan="2"></td></tr>
<tr><td>单元描述</td><td colspan="2">Here, we demonstrate quantum dots-hydrogel integrated gratings for actively switchable unidirectional emission with simultaneously a narrow divergence angle less than 1.5° and a large diffraction angle greater than 45°</td></tr>
<tr><td rowspan="2">结构单元图</td><td colspan="2">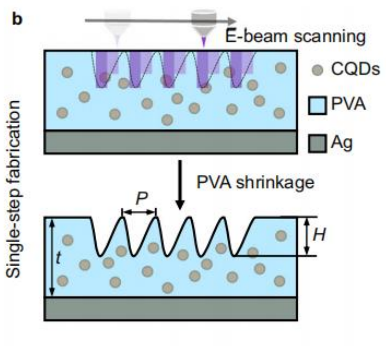
</td></tr>
<tr><td colspan="2">b) Schematic of the single-step fabrication of Q-HIG using grayscale e-beam lithography</td></tr>
<tr><td rowspan="2">指标</td><td>1 反射的角色散分辨率</td><td>2 测量1800纳米周期超表面的宽带角度分辨反射</td></tr>
<tr><td>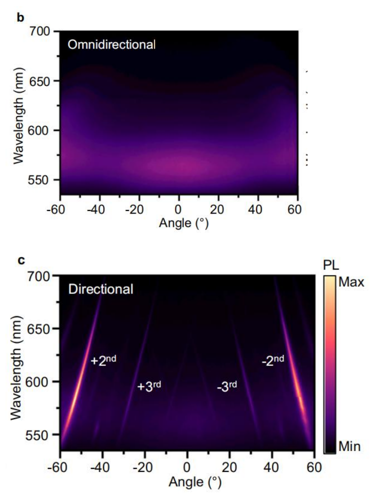
</td><td>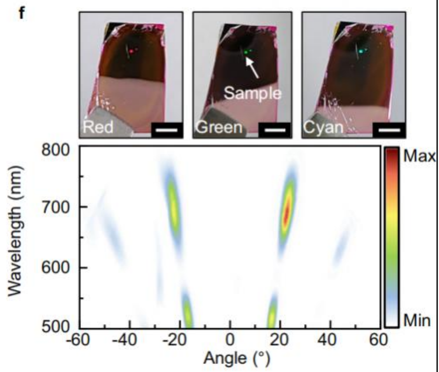
</td></tr>
</table>

		b, c Measured angle-resolved dispersion diagrams of PL emission from PVACQDs (b) thin film and (c) grating, respectively	f Measured broadband angle resolved reflection of the grating with an 1800-nm period. The top photograph scaptured under different shooting angles show the angular dispersion of the grating.
		3 不同波长下的增强值和散度角	
		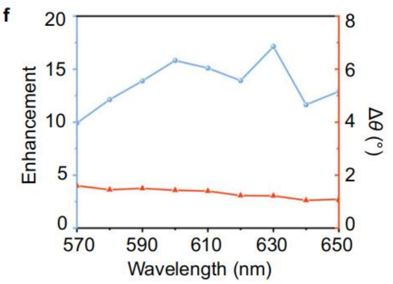	
		f Calculated enhancement（为衍射阶下光栅的 PL 强度除以相同角度下薄膜的 PL 强度）and divergence angle Δθ of the directional PL emission（发射角的半最大值处的全宽来定义的）	

1. 不同的单元结构形状

（1）颗粒凸起阵列

下图 4 是蛾眼抗反射结构模型[7]。就可见光范围，其透过率对于波长敏感，随波长的增加而增加；颗粒高度、直径大小都会影响透过率大小，总体上呈现间隙（周期距离与颗粒直径之差）增大而降低的趋势。透射谱变化明显时的波长范围和颗粒间隙、直径大小相匹配。

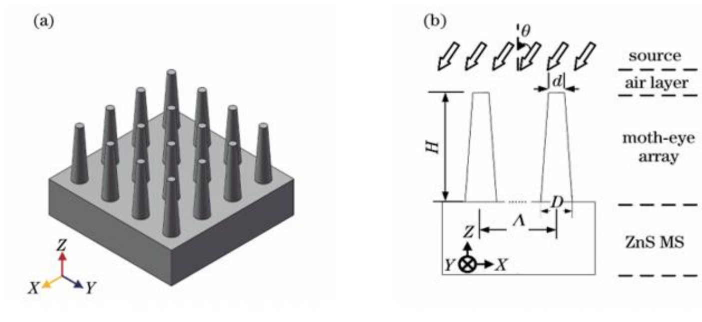

图 4 蛾眼抗反射结构模型 (a)三维结构模型 (b) 仿真模型示意图

下图 5 是金属纳米颗粒阵列[8]。如果颗粒周期相对颗粒直径太小，会降低不同单元透过率曲线的区别。此外，改变颗粒材料的 Ag、Au 比例会使得不同颜色色光的吸收率产生明显变化。其他相关论文也表明，在 50-200nm 范围内改变颗粒直径、在 200nm 左右改变排布周期对可见光的效果更好。不改变周期的情况下，增大颗粒直径、减小颗粒间隙能使反射谱红移。

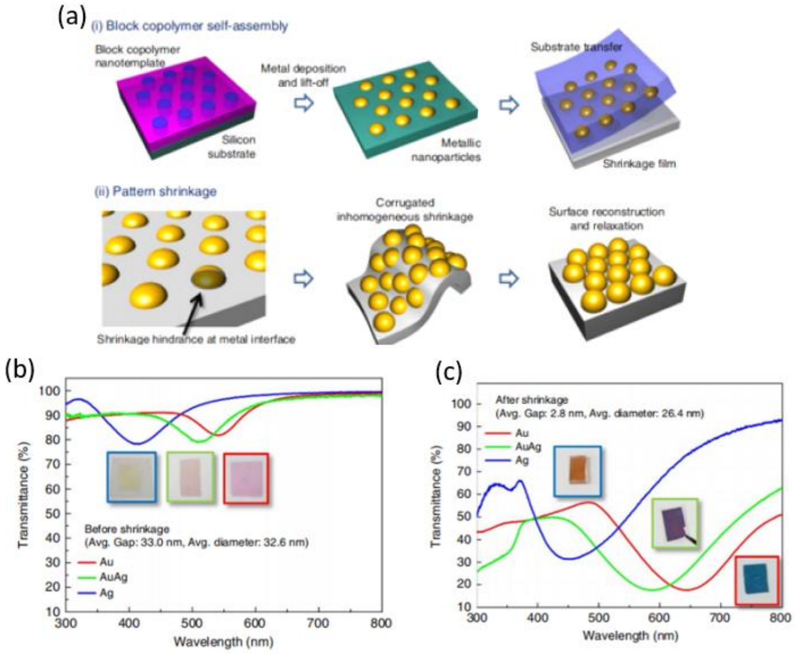

图 5 金属纳米颗粒阵列（a） 金属纳米颗粒系综图示 （b）超表面收缩前的透射光 （c）收缩后的透射光谱

（2）孔洞凹槽阵列：

下图 6 是一类紧凑的金属薄膜槽阵列[9]，以四个槽作为单元结构。槽本身的尺寸在 100nm 级别，但是周期尺寸达到了 600nm，其反射谱、透射谱在可见光范围内几乎不随波长响应。相对周期而言，单元结构尺寸对响应范围的影响不大。

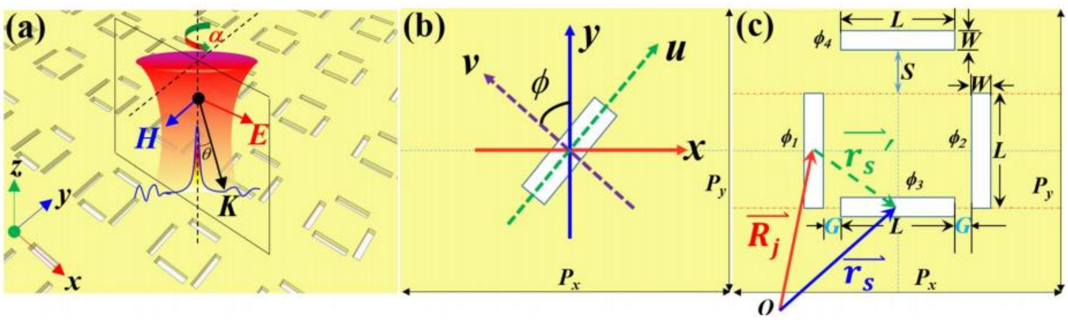

图 6 金属薄膜槽阵列（a） 金属薄膜凹槽阵列（b）矩形凹槽图示 （c）单元结构分布图

下图 7 是薄膜椭圆环 Ag 槽[10]。单元结构尺寸在 100nm 级别，周期 330nm，可见光范围内两个偏振方向的相移变化明显。图 7 说明。无尖角的槽也能改变相移和交叉偏振转化率。方形槽、椭圆形槽都具备明显效果。

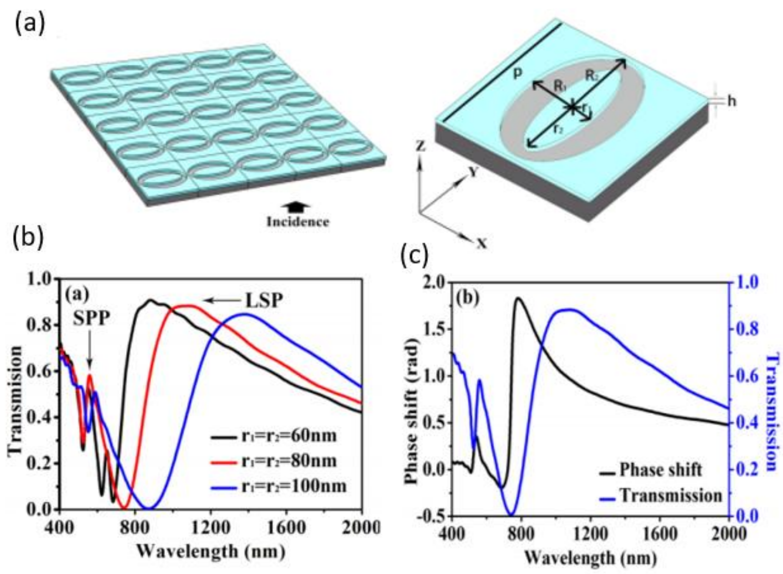

图 7 薄膜椭圆环 Ag 槽 （a）等离子体超表面 NCQW 结构示意图 （b）不同尺寸下的透射分布 （c）不同尺寸下的相移分布

（3）光栅结构

光栅周期一般设置在 300-1000nm 之间，都有良好响应。相比起光栅高度，改变占空比、薄膜折射率带来的反射光谱变化更大[11]。

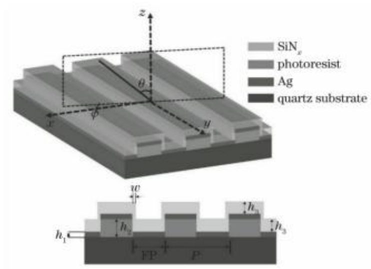

图 8 一维 Ag 薄膜周期反射光栅

2. 单元结构排布的变化性

相比仅含有一种单元结构的超表面，将形状、朝向、结构参数不同的单元结构集合组合成周期渐变型的超表面[12]（如图 9），能更方便地产生高纯度的色光。

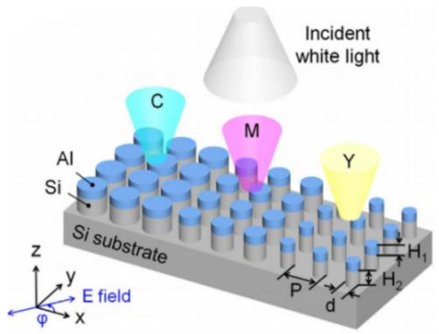

图 9 硅衬底上开发硅铝（Si-Al）混合纳米盘（ND）超表面

下图 10 是一个不规则排布案例，银颗粒阵列超表面[13]，由平均直径为 100nm 的不规则银纳米颗粒构成。其椭偏振幅系数和椭偏相移系数在可见光范围内都有明显的起伏。可见，

阵列颗粒就 100nm 量级而言，尽管直径大小不够统一，也可以有效地随入射角调控入射光信息。

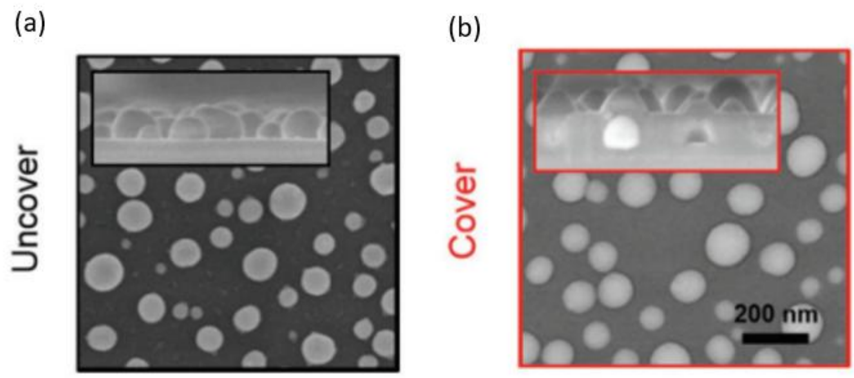

图 10 银颗粒阵列超表面 (a) 氧化物沉积前的超表面 (b)沉积后的超表面

3.超表面结构总结

要实现对可见光波长的响应，对于颗粒凸起状的单元结构阵列，把颗粒尺寸控制在 50-200nm 范围、把周期控制在 200nm 量级较为适宜，后者调节范围不宜过大。不同形状、甚至不规则的结构都可以实现明显调控效果，前提是控制好颗粒尺寸和周期。对于凹槽结构的超表面，则要控制好凹槽尺寸和周期，其大小要求和颗粒阵列类似。适当改变单元结构的排布朝向、形状、大小或者调节材料所用金属的比例，可以构造不同的像素点。

参考文献：

1. Cong, Longqing, et al. "All-optical active THz metasurfaces for ultrafast polarization switching and dynamic beam splitting." *Light: Science & Applications* 7.1 (2018): 28.
2. Baraldi, Giorgio, et al. "Self-Assembled Nanostructured Photonic-Plasmonic Metasurfaces for High-Resolution Optical Thermometry." *Advanced Materials Interfaces* 5.12 (2018): 1800241.
3. 罗蒙. "一种产生涡旋光束的勾型阵列超表面结构设计." *Laser & Optoelectronics Progress* 58.1 (2021): 108001-1.
4. 林鹤, et al. "宽光谱广角蛾眼抗反射超表面结构设计分析." *Chinese Journal of Lasers* 46.1 (2019): 113002-1.
5. 刘慧敏, 陈德利, and 孙晓红. "基于梯形结构的超表面透镜特性." *Laser & Optoelectronics Progress* 59.17 (2022): 1722003.
6. 宋志, et al. "反射型光变色超表面滤光结构." *Acta Optica Sinica* 41.20 (2021): 2023001.
7. Zhang, Jihua, et al. "Plasmonic metasurfaces with 42.3% transmission efficiency in the visible." *Light: Science & Applications* 8.1 (2019): 53.
8. Liu, Jie-Tao, and Zhi Liu. "Robust tunable plasmon induced transparency in coupled-resonance finite array of metasurface nanostructure." *Scientific Reports* 11.1 (2021): 1221.
9. Qian, Qinyu, et al. "None sharp corner localized surface plasmons resonance based ultrathin metasurface single layer quarter wave plate." *Scientific Reports* 11.1 (2021): 8956.
10. Yue, Wenjing, et al. "Subtractive color filters based on a silicon-aluminum hybrid-nanodisk metasurface enabling enhanced color purity." *Scientific reports* 6.1 (2016): 29756.

11. Smalley, Joseph ST, et al. "Subwavelength pixelated CMOS color sensors based on anti-Hermitian metasurface." *Nature communications* 11.1 (2020): 3916.
12. Gao, Renxian, et al. "Gigahertz optoacoustic vibration in Sub-5 nm tip-supported nano-optomechanical metasurface." *Nature Communications* 14.1 (2023): 485.
13. Kim, Ju Young, et al. "Highly tunable refractive index visible-light metasurface from block copolymer self-assembly." *Nature communications* 7.1 (2016): 12911.
14. Kim, Inki, et al. "Pixelated bifunctional metasurface-driven dynamic vectorial holographic color prints for photonic security platform." *Nature Communications* 12.1 (2021): 3614.
15. Su, Hang, et al. "Liquid-crystal-based electrically tuned electromagnetically induced transparency metasurface switch." *Scientific reports* 7.1 (2017): 17378.
16. Khaidarov, Egor, et al. "Large-scale vivid metasurface color printing using advanced 12-in. immersion photolithography." *Scientific Reports* 12.1 (2022): 14044.
17. Dai, Chenjie, et al. "Switchable unidirectional emissions from hydrogel gratings with integrated carbon quantum dots." *Nature Communications* 15.1 (2024): 845.